

# Entropy mediated organization of *E.coli* chromosome in fast growth conditions

Shreerang Pande<sup>a</sup>, Debarshi Mitra<sup>a</sup>, and Apratim Chatterji<sup>a,2</sup>

<sup>a</sup>Department of Physics, IISER-Pune, Dr. Homi Bhabha Road, Pune, India-411008.

This manuscript was compiled on April 6, 2023

**Recent experiments have been able to visualise chromosome organization in fast-growing *E.coli* cells. However, the mechanism underlying the spatio-temporal organization remains poorly understood. We propose that the DNA adopts a specific polymer topology as it goes through its cell cycle. We establish that the emergent entropic forces between polymer segments of the DNA-polymer with modified topology, leads to chromosome organization as seen *in-vivo*. We employ computer simulations of a replicating bead spring model of a polymer in a cylinder to investigate the problem. Our simulation of the overlapping cell cycles not only show successful segregation, but also reproduces the evolution of the spatial organization of the chromosomes as observed in experiments. This manuscript in addition to our previous work on slowly growing bacterial cells, shows that our topology-based model can explain the organization of chromosomes in all growth conditions.**

bacterial chromosome organization | entropic organization of bead-spring model of polymers | polymers in confinement |

It is vital for the living cell to make a copy of its DNA, and segregate it to two halves of the cell, before the cell can divide (1, 2). These essential processes have been extensively studied for the one of the simplest single celled organism, the *E.coli* bacteria. As the chromosomes replicate and segregate thereafter, the mechanism of spatio-temporal organization of the chromosomes remains controversial (3–9). Unlike in higher organisms, the bacterial cell does not have dedicated protein machinery to transfer its two daughter chromosomes to two halves of the cell (10). *E.coli* is a rod shaped bacteria, whose chromosome occupies the central region named the nucleoid. The bacteria does not have a nucleus. The segregation of the daughter chromosomes happens simultaneously as replication is in progress (2). In contrast, in eukaryotes, segregation of daughter chromosomes by the mitotic spindle occurs after replication is complete. Most bacterial cells have just one chromosome, and each chromosome is a ring polymer (11). The chromosome of the bacteria *E. coli* and *C.crescentus* consist of a single ring polymer with 4.6 million and 4 million base-pairs (BPs), respectively (12–14).

In *E.coli* and other bacteria, replication begins at a site called *oriC* to end at the *dif* locus of the *ter* macrodomain and proceeds along the two arms of the ring polymer simultaneously (5, 7, 15). Approximately 1000 base pairs (BPs) are replicated per second on an average, by the replication forks (RFs), moving along each arm of the chromosome (16, 17). By controlling the growth medium, the doubling time  $\tau$  of the *E.coli* bacterial cells can be varied to as low as 20 minutes to 3 hours or more (18). The cell cycle typically consists of three periods. The B period refers to the time period between the birth of the cell and the start of replication. Once replication starts, the cell enters the so called C period, and lasts till the time it takes for the replication to be completed.

Thereafter, the cell remains in D phase till cell division occurs (18, 19). The bacterial cells are said to be under fast growth, if  $\tau < \tau_C + \tau_D$ , where  $\tau_C$  and  $\tau_D$  refer to the C and D periods, respectively.

In fast growing cells, the B period is absent implying that the cells are continuously replicating and segregating. The conundrum of how a cell can divide in 20 minutes, even though the minimum replication time is 40 minutes was resolved by Helmstetter and Cooper and others (18) who showed that a daughter cell is newly born with partially replicated grand-daughter DNA. Thus a second round of replication begins even before the first round of replication is complete. Thereby, it is possible for the daughter cell to complete the rest of the replication (and segregation) of the grand-daughter DNAs thereafter, to divide into two grand-daughter cells in a time interval less than  $\tau_C^{min} = 40$  minutes. Refer Figure 1, for a schematic of how the multiple rounds of replication proceeds with overlapping cell cycles. Thus, the chromosome in fast-growth conditions undergoes multi-fork replication with the process of replication occurring simultaneously at more than two replication forks (18, 20).

It is accepted that for *E.coli* chromosomes, entropic forces between the ring polymers play a significant role in the segregation of daughter chromosomes (12, 21–27), though proteins like MukBEF also play a critical role in the process (6, 28). Moreover, researchers have used Fluorescent In Situ Hybridization (FISH) experiments to track the position multiple DNA-loci at different points in the cells life cycle, i.e. while the replication and segregation of the bacterial chromosome is in progress

## Significance Statement

*E.coli* cells grow with overlapping cell cycles in all but the slowest growth conditions. The fast growing bacteria can have four or more copies of the replicating DNA of different lengths. This makes the spatial segregation and the subsequent organization of the DNA a difficult task with two rounds of replication going on simultaneously. We show how the principles of entropy maximization of topologically modified confined ring DNA-polymers can achieve this. The topology is modified by introducing cross-links (emulating the effects of linker-proteins) between specific segments. Our simulation reproduces the emergent organization of chromosomes as seen *in-vivo*. Thus polymer physics principles, previously used to understand chromosome organization in slow growing *E.coli* cells, also resolves DNA-organization mechanisms in more complex scenarios.

SP implemented the model, performed calculations and analysis. The research plan was designed and discussed by SP, DM, AC. SP, DM and AC wrote the paper.

<sup>2</sup>To whom correspondence should be addressed. E-mail: apratim@iiserpune.ac.in

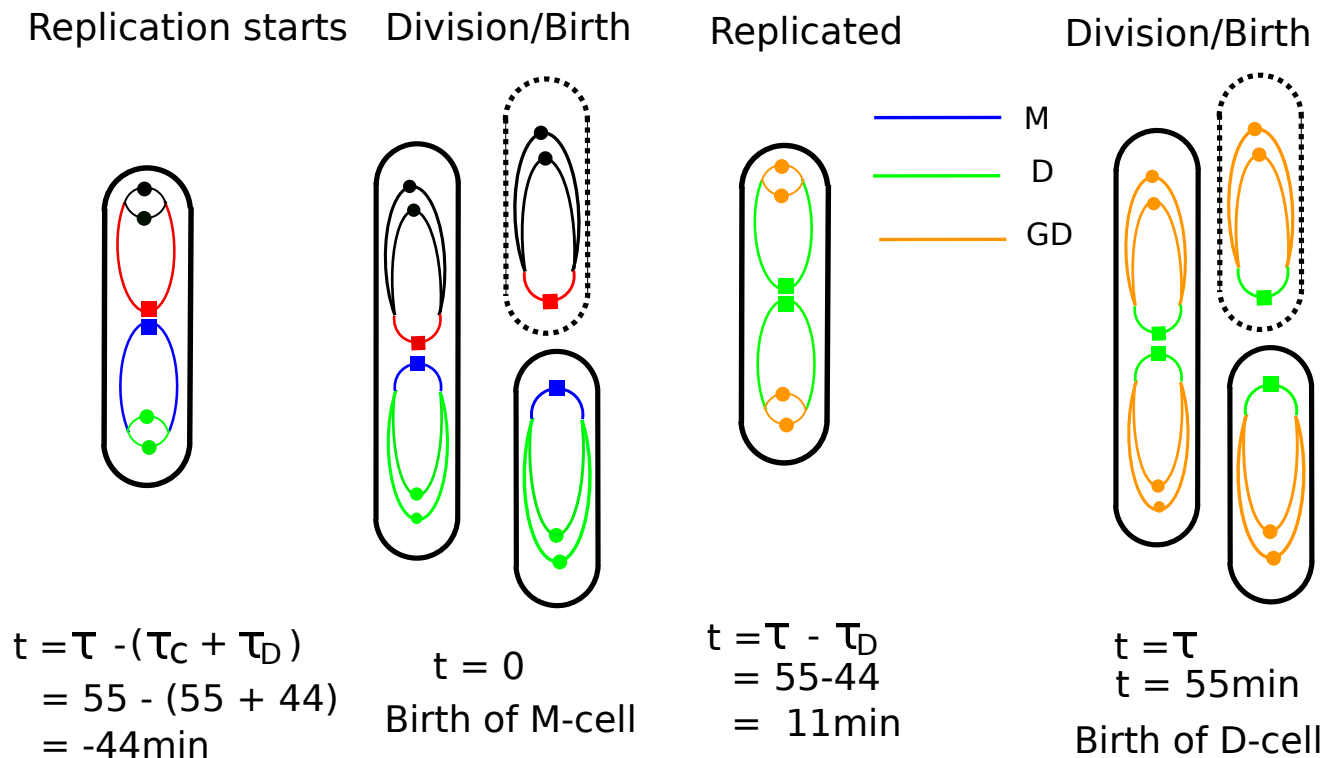


**Fig. 1. Schematic of the cell cycle:** Given a specific growth medium and other parameters, the E-coli grows with different C and D periods and doubling time  $\tau$ . In the specific case of the experiments that we are modeling (20), the C-period is  $\tau_C = 55$  minutes (min), and the D-period is  $\tau_D = 44$  min. This implies that the total time taken for a daughter chromosome to be produced by replication, and thereafter post segregation be part of a new daughter cell is 99 minutes (min). The cells are in fast growth conditions with overlapping cell cycles, thereby, the doubling time  $\tau$  is also 55 min. We explain the scenario explicitly in the figure for the benefit of the reader. In the schematic, a round of cell division takes place at time  $t = 0$ . This implies that after another  $\tau = 55$  mins, i.e. at  $t = 55$  mins, another cell division will take place to form daughter cells from the mother, as shown. We set the convention that the cell born at time  $t = 0$  is called the Mother cell (M-cell) and the cells born at  $t = 55$  mins is the Daughter (D-) cell. However, for the pair of daughter-chromosomes (green) which divide into the two D-cells at  $t = 55$  min, their replication started  $\tau_C + \tau_D = 99$  minutes earlier. This implies that the two (green) *oriCs* of the D-chromosomes were formed 99 minutes before the birth of the two D-cells, i.e. at  $t = -44$  mins. Let's follow the "green" chromosomes from the start of replication at time  $t = -44$  min. The *oriC* of blue chromosome in the grandmother-cell (GM-cell) starts a new round of replication at  $t = -44$  mins to form two green *oriCs*. The two RFs will start moving along the arms of the blue chromosome to form two complete green chromosomes after  $\tau_C$  mins, i.e. at  $t = 11$  mins. Meanwhile, the GM cell has divided to form two M-cells at  $t = 0$ , and we follow the cell which has the green chromosome. The other M-cell (shown in dashed line) have the red (& black) chromosomes, which are fully equivalent to that of blue (& green) chromosomes. But we color it differently to distinguish it from the green chain. Note that at time  $t = 0$ , the M-cells are newly born with with only 20% of blue chromosome (M-chromosome) and 80% green D-chromosome. From  $t = 11$  to  $t = 55$  mins (D-period), we have two green *dif-ters* connected to each other before cell division at  $t = 55$  mins. Moreover, at  $t = 11$  mins, the four new orange *oriCs* have formed from the two green *oriCs*, as a new round of replication starts. The D-cells are born with only 20% green D-chromosome and a pair of 80% formed orange grand-daughter chromosomes. In legends, we show the colors of the M (blue, red), D (green, black), GD (orange) chromosomes. To visualize the different stages of the cell-cycle the reader may refer to the section titled 'Movies' in the SI (videos 'Vid-1' and 'Vid-2').

both in fast and slow growth conditions (20, 29, 30). For slow growth, it is observed that the *oriC* is initially found in the mid-cell position, and after about 20 minutes into the C-period the two *oriCs* move to the quarter and three quarter positions along the cell-long axis (29, 31). The position of the *oriCs* are measured from one of the pole positions. Correspondingly, the *dif-ter* locus remains delocalized within the cell at the start of C period, but eventually moves to the mid-cell position at the end of the replication process. Other loci also move to their respective 'home positions' as segregation proceeds (29). The mechanism by which the different genomic loci identify their cellular addresses within the cell and then move to that position at the appropriate time of the cell-cycle remained an open question. In our previous work with slow growth conditions, we showed that this DNA-organization is obtained by the adoption a suitably modified polymer topology by having long range contacts, which are mediated by MukBEF or *rrn*-operons acting on the DNA-contour (31). As a consequence internal loops of the polymer segments are formed.

The different loops entropically repel each other and occupy different segments of the cell along the long axis, and thereby also localize different loci which are part of the loop.

In fast growth conditions with multifork replication, the existence of four (or more) chromosomes at different stages of the replication process makes the segregation and faithful division of chromosomes a more complex task. If there existed an active machinery which directs the newly replicated chromosomes to opposite directions to segregate them, then the daughter and the mother chromosomes might end up being spatially overlapped, in this complex life cycle (20). It is because if there are overlapping rounds of replication that take place and each chromosome (of each generation) must move in appropriately different directions such that they occupy a specific region in the cell, without being spatially proximal to the chromosomes of the previous/subsequent generations. Therefore, an entropic model without any active-segregating machinery which achieves the purpose can be a lucrative idea with a minimal number of assumptions. The question how-

ever is, does the same entropic mechanism which explains loci-organization in slow growth also explain the organization of segregating chromosomes in fast growth? In this paper, we establish that it is indeed the case and demonstrate that the same mechanism can also be used to obtain the organization of loci along the cell long axis in fast growth conditions with overlapping replication cycles, and establish quantitative consistency with previously published experimental data (20). Thus our proposed mechanism is likely a generic mechanism to obtain chromosome organization in bacterial DNA, as we have also previously quantitatively matched our model results with organization of loci as shown by HiC and FISH data for the chromosome of bacteria *C. crescentus* (32).

**Model and mechanism:** We use the bead spring model of a polymer with 500 monomers to model a single chromosome (with 4.6 million base pairs) within a cylinder, while multifork replication is in progress. The cylinder length doubles in small steps over the course of the simulation while the diameter remains fixed as observed for *E. coli* cells *in vivo*. The length  $a$  of the springs connecting the centers of neighbouring beads is the unit of length, and a polymer is confined within a cylinder of diameter  $7a$  ( $\equiv 1\mu\text{m}$ , the typical diameter of the cell), and the cylinder length increases doubles from  $21a$  ( $\equiv 3\mu\text{m}$ ) to  $42a$  as our simulation proceeds. We use Monte Carlo (MC) simulations to update the position of the monomers, where one Monte Carlo step (MCS) consists of  $N$  attempts to update the position of the  $N$  monomers, chosen at random. Since we model replication and thereby add monomers at the RFs at regular intervals,  $N$  keeps increasing as the simulation proceeds. To update monomer positions, a trial move is made to displace the monomer in a random direction, and the move is accepted or rejected using the Metropolis criterion and depends on the resulting energy change, choosing  $k_B T = 1$ . The polymer keeps changing conformation as simulation proceeds as the monomers undergo local diffusive motion. A description of the model can be found in (31). We suitably adapt our previous model for fast growth conditions, refer Supplementary information SI-(1-3) for details.

For our previous study (31) in slow growth conditions, we had introduced chromosomal loops by bridging specific loci along the chain contour of daughter DNAs, after the RFs had crossed the corresponding loci of the mother DNA. These loops are created in our simulations by introducing additional springs which cross-link between specific pair of monomers along the chromosome contour. These cross-links (CLs) mimic the role of bridging proteins (8), such that distant genomic segments become spatially proximal. A loop or an internal ring is formed by the DNA-segments which lies in between the specific loci. These internal loops entropically repel each other, which implies that each loop can take a larger number of conformations if they do not overlap with each other. Thus configurations where there is minimal overlap between loops have lower free energy, assuming conditions of local equilibrium, though we are aware that a cell is energy consuming driven non-equilibrium system. This entropic repulsion between loops consequently induce the loops to occupy different segments of the cylinder along the long axis. Thereby one obtains emergent organization of the chromosome loci, which belong to particular loops. We posit that processes like loop extrusion make transient loops, which give rise to the TADs observed in the Hi-C maps, whereas some loops are more long lived

and give rise to the macro-domain structure of Hi-C maps. Consequently, these result in the spatio-temporal localization of tagged loci to points along the cell long axis.

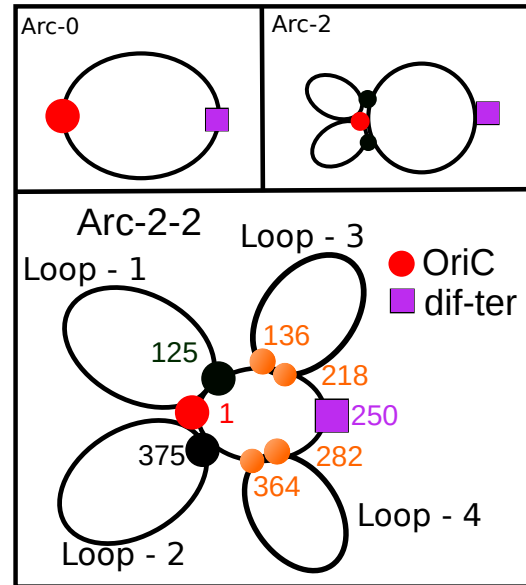


**Fig. 2. Schematic of the different architectures:**The schematic shows the Arc-2-2 topology of the DNA-polymer with 500 monomers. It is a ring polymer (Arc-0), thus monomer 1 is joined to monomer 500. We label monomer-1 as oriC and monomer 250 as dif-ter. In addition, we suggest that monomer 125 & 375 is cross-linked to monomer 1 by bridging proteins to create the Arc-2 architecture of the polymer. Two overlapping polymers in the Arc-2 architecture have enhanced forces of segregation, as compared to the ring polymer. In addition, they also show loci localization as seen in FISH experiments, but the contact map obtained from simulations only partially matched the HiC data of the *E. coli* chromosome. Additionally, if monomers 136 & 218, as well as 282 & 364 are cross-linked, we obtain the architecture named as Arc-2-2. Simulations with the Arc-2-2 architecture reproduced all the results obtained with Arc-2, and also showed macro-domain organization as seen in the HiC maps. In this manuscript, we use the same Arc-2-2 architecture to model mother and daughter chromosomes in cells with overlapping life cycles. Organization of tagged loci as seen in FISH experiments spontaneously emerges out from our simulations. In simulations presented in this paper, the daughter chromosomes are in the Arc-2-2 topology at time  $t = 0$  (refer Fig.1), whereas the grand-daughters adopt the Arc-2-2 topology, after the relevant monomers are replicated and become available for cross-linking by springs. *In-vivo*, we expect active processes contribute to bring the relevant segments in spatial proximity before they are bridged by the relevant proteins: these are not being modeled presently. Thus though the cross-linking is instantaneous after replication of specific monomers in our simulations, it will not be so *in-vivo*.

Previously, we used two polymer architectures named Arc-2 and Arc-2-2(31) to unravel the mechanism (32) of loci-organization in slow growth conditions, refer Fig.2. Moreover, though the RFs were made to move along the chain contour (train track model) as replication progressed, we observed that the RFs remain spatially localized near the cell center. This spontaneously emerges out in our simulations as a consequence of the chosen architecture. This is consistent with the replication factory model in spirit, and thus reconciles consequences from two contradicting models pertaining to the motion of RFs. In this paper, we use the same Arc-2-2 architecture for our model of replicating chromosomes to study organization in fast-growth conditions. We model the chromosome replication and segregation over one doubling time  $\tau$  inside a growing cylinder (*E. coli* cell). The simulation starts from the state right after cell division (equivalent to the state shown at time  $t = 0$  in Fig.1), such that two new cells are just born from



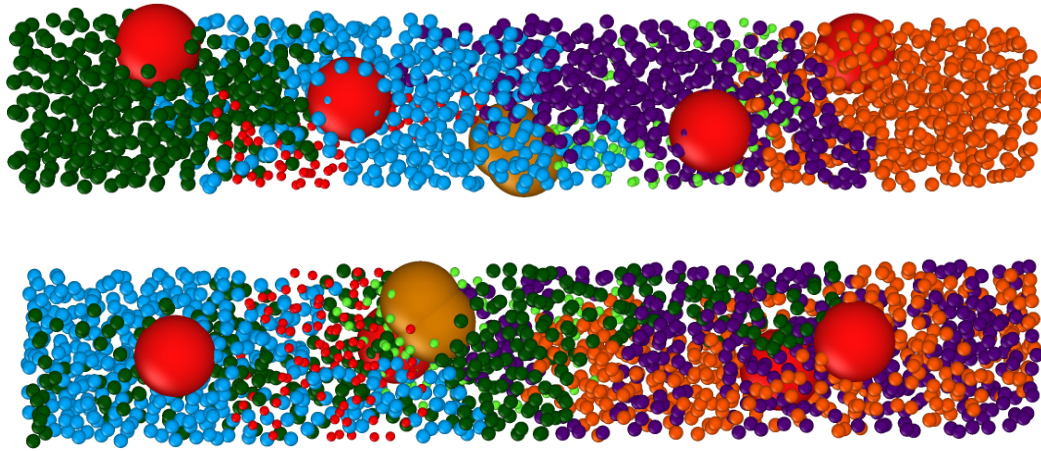


**Fig. 3. Snapshot of simulations for Arc-2-2 and Arc-0** Fig. shows representative simulation snapshots taken at the last stage of the cell-cycle before cell-division, for Arc-2-2(top frame) and Arc-0(bottom frame), polymer topologies. The green and red small spheres are the monomers of the daughter chromosomes. We note that for Arc-2-2 the grand-daughter chromosomes (shown in orange, violet, blue and deep-green) get spatially localized to specific regions along the long axis, while for Arc-0 the grand-daughter chromosomes show greater spatial overlaps with each other. The four big red spheres represent the four *oriCs*, whereas the two big orange spheres are the two *dif-ter* loci, they are connected to each other as is seen *in-vivo*.: they are of the same size as other monomers in the simulation. In the subsequent sections we show that loci show localization patterns for Arc-2-2 but Arc-0 show no such localization patterns.

their parent cell. We follow the replication of chromosomes in just one cell and the simulation ends just before the cell is ready to divide into two daughter cells. The newly born mother cell (M-cell) at  $t = 0$  has 80% partially replicated mother M-chromosome, i.e. there are two D-chromosomes (schematically) marked in green with 400 monomers each and 20% mother chromosome marked in blue with 100 monomers; refer Fig.1. Thereby, there are two *oriCs* at the start of simulations. Refer SI-2 for details of how we model replication, and SI-4 to know the details of how we initialise the system.

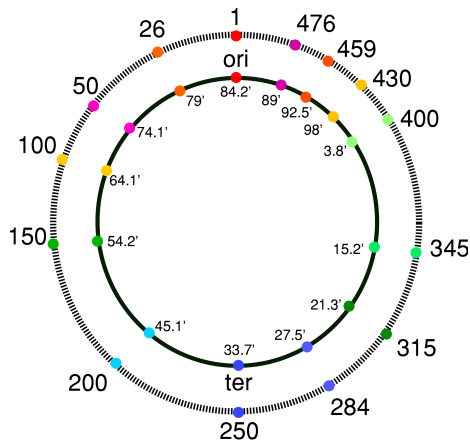


**Fig. 4. Schematic of the tagged loci:**Schematic of chromosome loci tagged in experiments and the corresponding monomer indices for a 500 monomer chain. Experimentally, the circular chromosome is tagged at different sections, where different loci along chain contour are denoted in terms of minutes and seconds. The inner circle in the schematic corresponds to the loci fluorescently labelled in the experiment (20). The outer circle denote the monomer indices corresponding to these labels in our model system, where the *oriC* is denoted by monomer index 1, and *dif-ter* by monomer index 250. As multifork replication proceeds, there can be more than one loci of a given label within the cylinder (cell) at a particular stage of the cell cycle.

During the course of our simulation, the two RFs reach the *dif-ter* loci such that the mother is completely replicated

to 2 green D-chromosomes and the cell enters the D-period. Simultaneously, a new round of replication starts such that the two (green) D-*oriCs* each divide into two (orange) GD-*oriCs*. The simultaneous start of the second round is a consequence of the choice of  $\tau$  and  $\tau_C$  in our model, which have been adapted from (20). For modeling replication, we add monomers at a fixed rate of 1 monomer every  $2 \times 10^5$  MCS at each RF. Moreover, to mimic the role played by topoisomerase within the living cell, we allow topological constraint release at regular intervals at rates we used previously, i.e. every  $10^4$  MCS. We track the position of all the (available) *oriCs* and other monomers as the simulation proceeds. We do not model cell division. We have also outlined the mechanism of topological constraint release in our simulations in SI-5.

Though we use Monte Carlo simulations for our investigation of chromosome organization as the cell goes through its life cycle, the simulation is quintessentially a Non-equilibrium simulation scheme. In the simulations, we (a) add effects of polymers chains crossing each other to release topological constraints, (b) add monomers to the simulation box at regular intervals at different points along the contour, i.e. at the position of the RFs to mimic replication and formation of two chains from one, (c) add cross-links at certain stages of the simulation, and lastly (d) increase the length of the cylinder as the simulation proceeds. These are energy consuming non-equilibrium processes inside the cell, and these steps break detailed balance in the simulation. MC is used primarily to model diffusion of monomers and the exploration of different conformations of polymers in a confined space, assuming local equilibrium (33, 34). While modelling the cell cycle, we do not map Monte Carlo Steps (MCS) directly to time in terms of minutes, but rather in terms of the stage of replication.

## 1. Results

**Localization of *oriC*, *dif-ter*:** As in experiments, we follow the trajectories of particular monomers along the chain contour as the cell cycle proceeds. These monomers correspond to the

same genomic loci which have been tracked in the experiments of (20), also refer Fig.4. We quantify organization by plotting their spatial distribution in five equally divided intervals of their life cycle, as in experiments. The probability distributions of the position of specific monomers at different stages of replication/segregation can be directly compared with data from experiments. The experimental data for specific genomic loci has been provided in Fig.5 (20) for ready comparison with data from simulations. We average our data over 50 independent runs corresponding to a life cycle in 50 cells.

As mentioned earlier, we start the simulations with the birth of a new cell corresponding to  $t = 0$  of Fig.1. It is known that the two replicated *dif-ter* loci remain linked to each other and are localized in the middle of the parent(M-cell) cell up to just before cell-division. To mimic this phenomenon in our model, we kept *dif-ter* monomer tethered to one of the poles of the cylinder (corresponding to the new pole of the cell), and release the tether just at the start of the simulation. Before we start our simulations, we equilibrate the two D-chromosomes connected at the two RFs (located at monomer indices 200 and 300, assuming completion of 80% replication on both arms) on the M-chromosome. The equilibration run is for  $3 \times 10^7$  MCS while allowing for topological constraint release. In this stage, we have the CLs which create Loop-1 and Loop-2 in each of the D-chromosomes, while the mother M-chromosome has the CLs which results in Loop-3 and Loop-4, refer Fig.2 and other details in SI-4. Note we model a life cycle where the ratio of the  $\tau_D/\tau_C = 0.8$  and  $\tau/\tau_C = 1$ .

Soon after the simulation starts, the *dif-ter* monomer (the 250-th monomer) will be near the end of the cylinder where it had been tethered during equilibration. Thus the probability distribution shows non-zero values near the ends of the cylinder in the first 20% of its life cycle. But even as the RFs move towards the *dif-ter* loci and cross the 218-th monomer, we introduce CLs between the newly introduced 218-th monomer and the 136-th monomers to form Loops-3 (and correspondingly Loop-4) for both the D-chromosomes. Two double helix DNA chains are formed from the leading and lagging strands *in-vivo*. However, such details are beyond the scope of our coarse grained model. We re-christen the monomers of the parent DNA as monomers of one of the newly replicated DNAs instead of introducing new monomers, after the RF has passed the corresponding loci of the parent. The monomers being added at the RFs form the other newly replicated DNA-polymer. Thus, in our model the two D-chromosomes keep elongating at the cost of the length of the M-chromosomes, as seen *in-vivo*. Refer SI-3 for schematic diagram to better understand how we implement the cross-linking in our simulations.

The entropic repulsion between the loops of the two D-chromosomes ensures the segregation of the two polymers into two halves of the cylinder. This also relocates the *dif-ter* loci to the middle of the elongating cylinder. As a consequence, we also observe a peak for the probability distribution of *dif-ter* at the middle of the cylinder at all stages of the life-cycle, refer first row of Fig.6. As the two D-chromosomes occupy two different halves of the cylinder, the *OriC* moves to the mid position of each half cylinder, i.e the quarter positions of the elongated cylinder, in the (0 – 0.2) and (0.2 – 0.4) stages of the cell life cycle, as seen *in-vivo*. This is due to the repulsion between internal loops within each D-chromosome.

This organization emerges spontaneously in our simulations as a consequence of the adoption of the Arc-2-2 polymer topology, as we show in the second row of Fig.6.

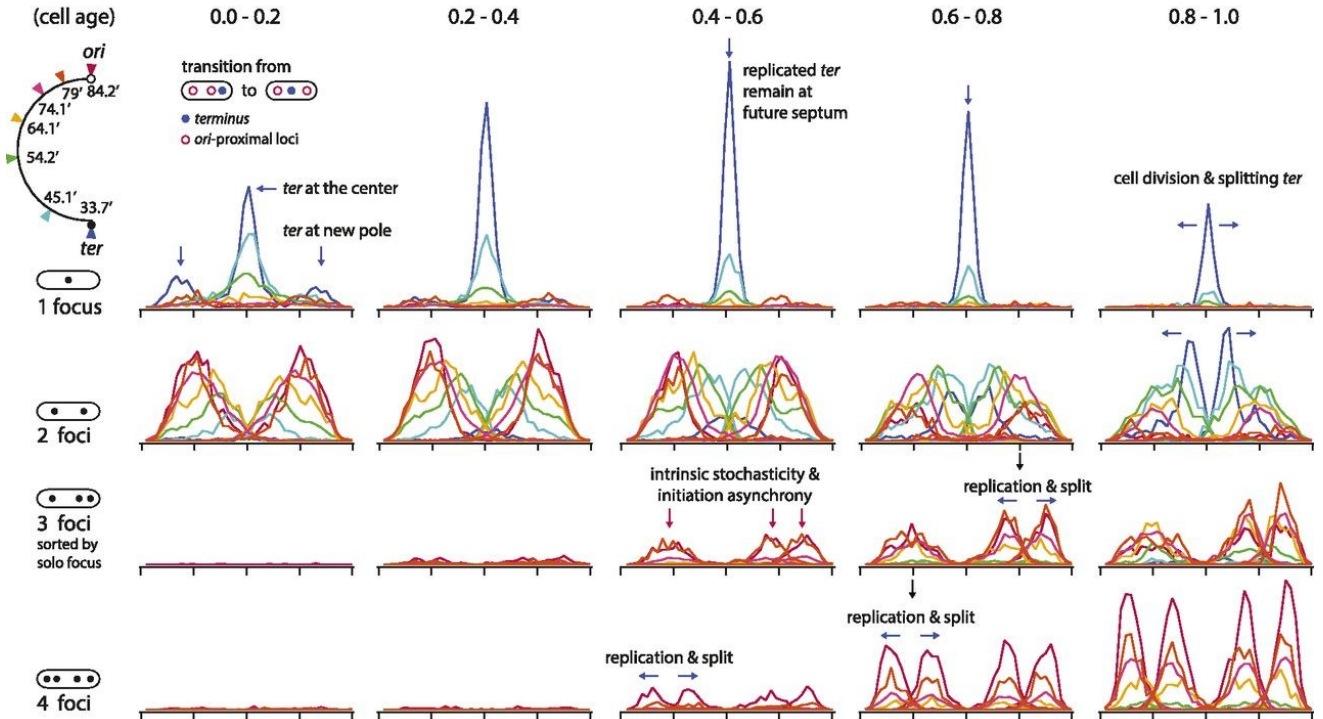
#### Comparing data from experiments & simulations:

Since the two D-chromosomes are connected at the *dif-ter*, the *dif-ter* continues to remain in the cylinder center. This continues even when the next round of replication starts at the two *oriCs* of the D-chromosomes. When comparing our results to that of experiments, there are some caveats related to conventions of presentation of data which need to be accounted for. Sometimes, these bring up apparent differences between the data obtained from experiments and our simulations, the reasons for which has been explained in subsequent paragraphs. For example, we don't see two peaks in the *dif-ter* distribution as we don't model cell division: compare the data in Fig.6 with the two-foci data in Fig.5 for (0.8 – 1) interval.

We have two *oriCs* till (0 – 0.2) interval in the cell life cycle, thereafter, there are four *oriCs* in our simulations. We can track the four *oriCs* independently and plot their spatial probability distributions in the last four interval of cell cycle. However, in experiments in the (0.2 – 0.4), the two just replicated *oriCs* cannot be distinguished in FISH data, since the newly replicated *oriCs* segregate after a certain interval of time, known as the cohesion time. Hence data for the spatial distribution of four *oriCs* do not appear till the 0.4 – 0.6 interval of life cycle. Consistent with the observation of cohesion time, the distributions of the *oriCs* overlap significantly in our simulations, in the 0.2 – 0.6 interval of the life-cycle. This overlap decreases as the *oriCs* localize. Furthermore in our modeling, we do not have a scenario with three *oriCs*. But *in-vivo*, one can observe 3 *oriCs* in the cell, because start of replication need not be perfectly synchronous (as in simulations). Moreover, segregation of the newly replicated *OriCs* may proceed at slightly different rates due to inherent stochasticity in the active process which govern cross-linking by binding proteins. This can give rise to different cohesion times for different pairs of replicated *oriCs*, which in turn can result in the observation of three *oriCs*. These reasons hold true also for the data of spatial distribution of other loci as presented later. Another important difference is that we can identify and track the loci of GD-chromosomes and the D-chromosome (shown in different colors), but experimentally one cannot distinguish between the two to identify whether a loci belongs to D or GD-chromosomes. In the experiments one can count the number of cells with two or three or four fluorescent foci, and plot their spatial distributions.

Furthermore, in simulations we observe spatial distributions for GD-*oriCs* to show relatively high occupancy values near the cylinder ends for the three intervals corresponding to 0.2 – 0.8 stages of the life-cycle, which is not seen in experimental data. This is because *in-vivo* the bacterial chromosome is condensed to stay to form a region called the nucleoid due to the presence of many other loops due to transient cross-links. These have not been incorporated in the current study. These transient loops will help shift the distributions away from the cell boundaries. However, in experimental plots we do observe rather broad *oriC* distributions for the 2 and 3-foci data in the 0.4 – 0.8 interval of cell-cycle; and even wider distributions in 0.8 – 1 interval for data with two foci, i.e. when the two foci cannot be distinguished. Thus, our results are not in contradiction to those obtained from experiments.

**A Cell long-axis histograms: information flows outward during multifork replication (except *ter*)**  
 (area under the curve reflects the fraction within the population; the color of the lines matches the chromosome marker.)



**A Replication forks (Ssb-GFP) at three narrow zones of segregation**  
 (all age classes; area under the curve reflects the fraction within the population)

**B Splitting chromosomal loci positions**  
 (all age classes)

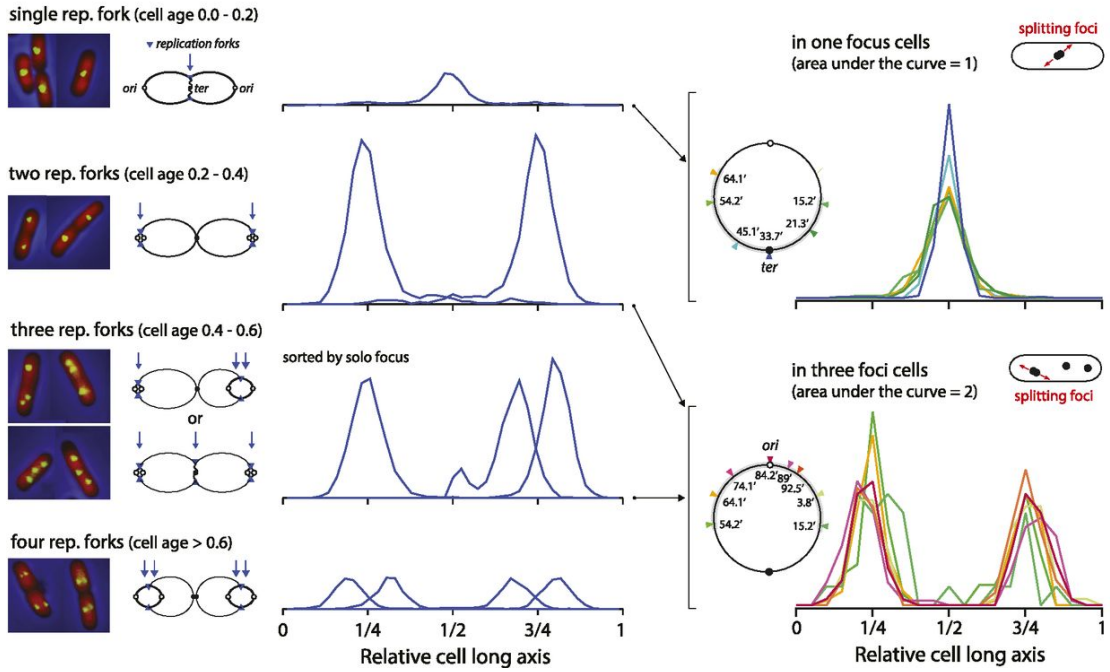


**Fig. 5. Experimental data of the modelled system:** This figure has been adapted from previously published data in (20) (after having obtained requisite permissions) for aid of comparison with our results, presented in Fig. 6 and Fig. 7. The data shows frequency distributions for different fluorescently tagged loci at different stages of the cell cycle. Other details can be found in the text and in (20)



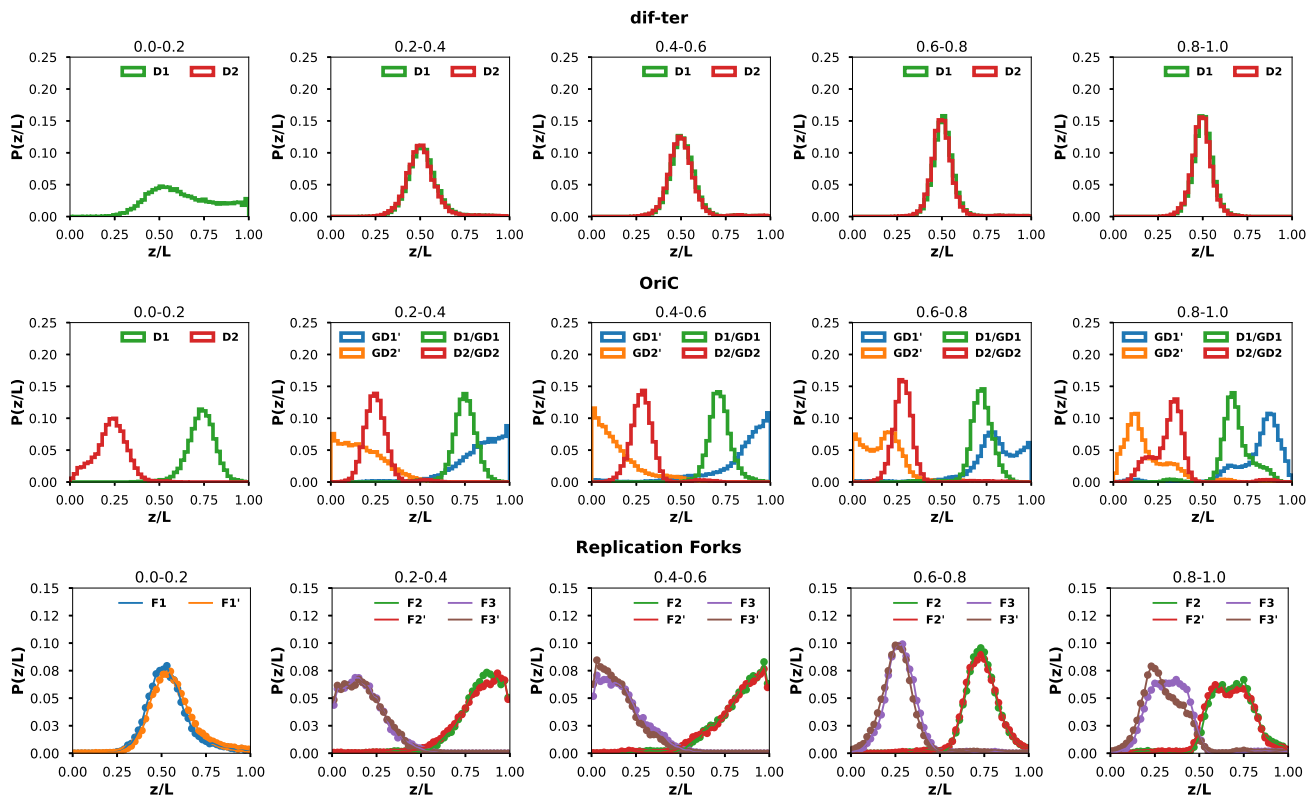


**Fig. 6. Long axis distributions for *dif-ter*, *oriC* and the replication forks:** We plot the spatial probability distributions ( $P(z/L)$ ) of the position of different loci, where  $z$  denotes the position along the long axis of the cylinder (cell), and  $L$  is the length of the cylinder at that stage of the simulation run. Data is shown for *dif-ter* locus (first row), *oriC* locus (second row) and the RFs (third row) for various intervals during the life cycle. The intervals are indicated at the top of each subfigure. In the first interval, there are only two data sets corresponding to the loci of the D-chromosomes. Thereafter, in subsequent intervals one may observe the spatial distribution data corresponding to both D and GD chromosomes, depending on when (and whether) that particular locus gets replicated. Once a particular locus gets replicated then the corresponding D monomer is renamed as the GD monomer (eg: D1 is renamed to GD1), and new monomers have also been introduced due to the replication protocol (labelled GD1'). The distribution for the renamed GD monomer (eg: GD1) is normalised by a different number, as compared to the GD monomer that was recently introduced (i.e. GD1'). The normalization is different because the GD1 monomer was already present as the D1 monomer, even before it was replicated. The same labelling and normalization protocol holds true for D2, GD2 and GD2' monomers. The *dif-ter* locus gets replicated once. In the stage corresponding to  $0 - 0.2$  we have only the D1 *dif-ter* locus. In the next stage the D1 locus has been replicated and there are two overlapping distributions corresponding to D1 and D2 (which remain cross-linked). The *oriC* locus gets replicated at the start of the  $(0.2 - 0.4)$  interval and hence the plots show four different data sets. The localization of the *oriCs* and the *dif-ters* can be visualized from our representative simulation video 'Vid-3' (refer SI, section 'Movies'). In the third row we plot the spatial distributions of the RFs as they are assumed to move from one monomer to the next, along the chain contour. In the  $(0 - 0.2)$  interval there only two RFs which move along the contour of the M-chromosome (shown in orange and blue). Thereafter, one has four RFs branching out from the two *oriCs* of the D-chromosomes, which get replicated to form the GD chromosomes. Note that GD1 and GD1' chromosomes occupy one-half of the cell while GD2 and GD2' occupies the other half. In the third row we show the spatial distributions of the RFs in different intervals of the life cycle. The RFs have been named in a specific way to clearly demarcate those which are traversing along different arms of the same chromosome. For instance, RF1 and RF1' are the two replication forks moving along the two arms of the mother chromosome, while RF2 and RF2' denote the RFs moving along D1 and corresponding RF3 and RF3' moving along D2.

In simulations, the CLs between the 125-th and 375-th monomer and the *oriC*, are already present for two of the GD chromosomes, as they have been rechristened from the D-chromosomes. In the two other GD chromosomes, CLs are being introduced in this stage of the life cycle, once the relevant monomers get replicated. This happens when the RFs proceed beyond the 125-th (and 375-th) monomer in the  $0.6 - 0.8$  life-interval in our simulations. Thereafter, one has four GD-chains each with Loop-1 and Loop-2. As this occurs in the middle of  $0.6 - 0.8$  stage of the life cycle, the two *oriCs* start to occupy the  $1/8$  and  $3/8$ -th positions in one half of the cell. Correspondingly, the other two *oriCs* in the other half of the cell occupy  $5/8$ -th and  $7/8$ -th positions, leading to the appearance of four peaks at these positions. This is seen *in-vivo* and in our simulations, and the localization occurs due to entropic repulsion between GD-loops. The peaks are enhanced in the next stage of life cycle.

**Position of Replications Forks (RFs)** The confidence in our model is further strengthened by the reconciliation of the spatial distribution of the RFs from our model and *in-vivo* results. We have all the positional information of the position of the model RFs as we know the position of the RFs on the chain contour at different stages of the cell's life cycle; refer 3-rd row of Fig.6. In the  $(0 - 0.2)$  stage, the two RFs on the M-chromosome move from the 200-th (and the 300-th) monomer to the *dif-ter* position. Thereby there is a peak in the spatial distribution at the center of the cell, which the *dif-ter* itself gets to occupy after cell division due to reasons already explained. At the end of the  $(0 - 0.2)$  interval, the replication of the M-chromosome is complete and one has two complete D-chromosomes connected at the *dif-ter* in the Arc-2-2 architecture. The Arc-2-2 architecture ensures that the *oriC* are in the quarter positions, as the two D-chromosomes occupy different halves of the cell (31).

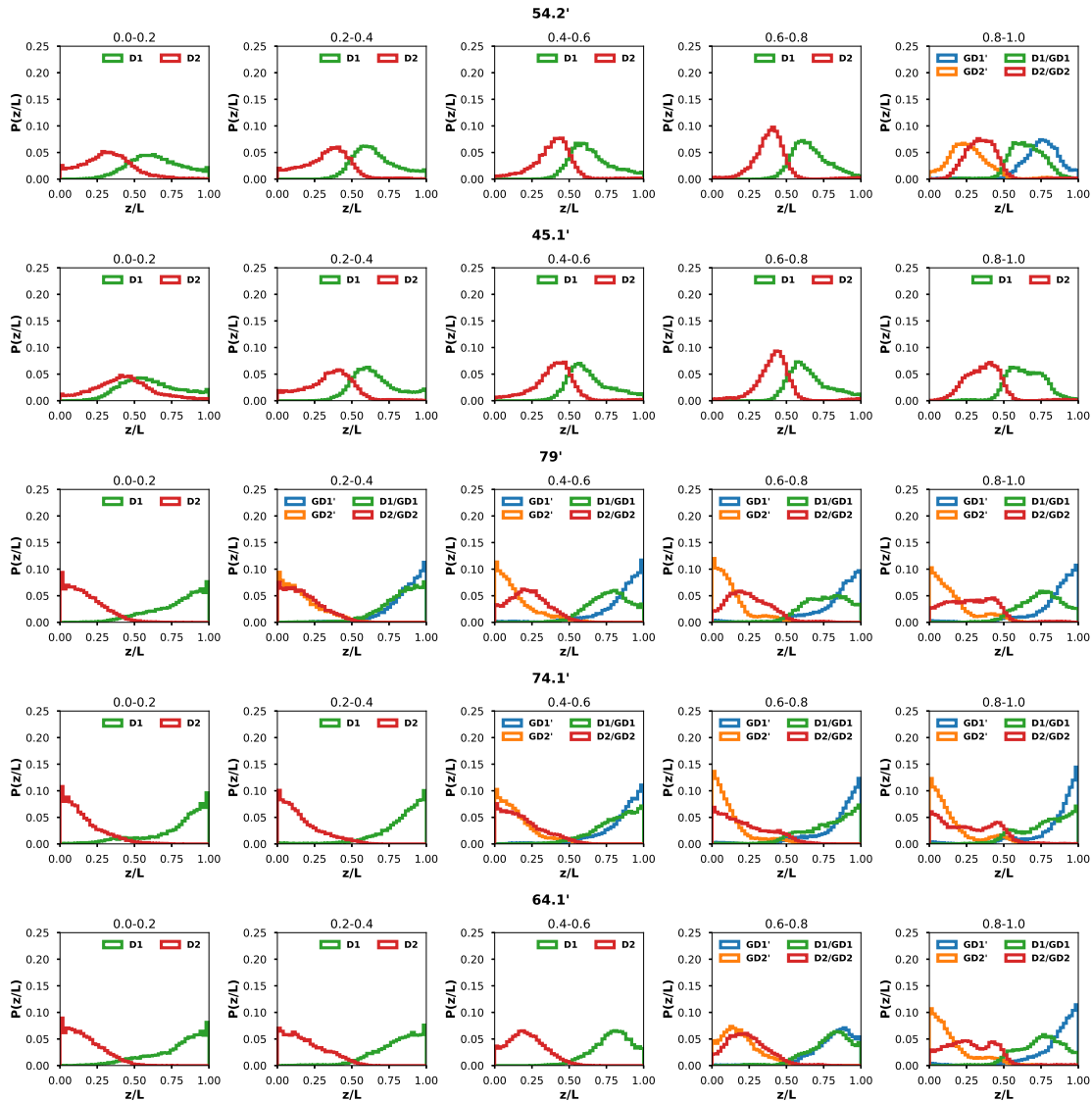


**Fig. 7. Long axis distribution for other tagged loci:** We plot the spatial probability distributions ( $P(z/L)$ ) of the position of different loci, where  $z$  denotes the position along the long axis of the cylinder (cell), and  $L$  is the length of the cylinder at that stage of the simulation run. Data is shown for 54.2' locus (first row) and for 45.1' locus (second row), 64.1' locus (third row) and 74.1' locus (fourth row), during the life cycle. The corresponding monomer indices are at the top of each row. The other plotting conventions are same as in Fig.6.

At the start of (0.2 – 0.4) interval, replication of each of the two D-chromosomes begins from the two *oriCs*. Thus four new RFs start at the position of the *oriCs* to start creating the GD-chromosomes. Thus, they start out from a position close to the quarter positions as reported for experimental data obtained *in-vivo*. Thereafter, the RFs start moving along the the two arms as in the train track model. Their positions are maintained around the quarter position as the cell elongates, though they also get pushed out towards the cylinder ends by the unreplicated sections of D-chromosomes. Because of the reasons mentioned above, the GD-*oriCs* are closer to the cell-ends in the simulation, thereby RFs show higher propensity to be in cell-ends in the (0.2 – 0.6) stage, though it peaks near the quarter positions as in experiments.

The spatial distribution of RFs can again be observed and understood in the (0.6 – 0.8) interval from Fig.6, as they move away from the *OriCs* along the contour towards the sites of

CLs ( monomer 125 and 375) which make up Loop-1 and Loop-2. The CLs will be formed by linking monomer pairs (1 – 125) and (1 – 375), and thus after the CLs have formed at time  $0.7\tau$ , the RFs will be spatially proximal to the *oriCs*. After the Loop-1 and Loop-2 of GD1' (and correspondingly GD2') are formed at  $0.7\tau$ , the *oriCs* of the GD-chromosomes move to the 3/8-th and 5/8-th positions. Thus the RFs will also be found at this position.

In the last (0.8 – 1) interval of the cell cycle, as the RFs move towards *dif-ters* of the two D-chromosomes, starting out from the CL sites, as mentioned in the previous paragraph. Thus, there is a higher propensity for them to be near the cell-center, but there are indications of some spatial separation along the long axis in the position of two RFs, in the data from our simulations as seen in Fig.6 3rd row. In contrast, the experimental data for cell-age  $> 0.6$  in Fig.5 clearly shows a prominent separation of peaks in the spatial distribution



of RFs. To check the reason for this discrepancy of our data (averaged over 50 runs) from experimental data, we plot the spatial distribution of the RFs from individual runs in the  $(0.8 - 1)$  interval of the life cycle: refer SI-6 for data on spatial positions of RFs from 50 individual runs. Many of these clearly show 3 to 4 peaks. Note that when we plot the averaged data shown in Fig.6 (3rd row), the separation of the peaks diminish, since the positions of the RFs can be oriented differently relative to each other, across different simulation runs. We compared the spatial distribution of RF data obtained with Arc-2-2 with that obtained using the Arc-2 architecture in SI-6 and SI-7 respectively. In comparison, the data obtained using Arc-2 architecture shows lesser separation between the peaks, which indicates that Loops-3 and Loops-4 (absent in Arc-2 architecture) play a role in the separation of peaks, seen in the spatial distribution of RFs.

Next, to find the relevant correlations, we plot the spatial distributions of center of mass (COM) of Loop-3 and Loop-4 in interval  $(0.8 - 1)\tau$  SI-8, and compare this distribution with the distribution of RFs for Arc-2-2 architecture. We do this because at this stage of the life cycle the RFs are traversing along the contours of Loop-3 and Loop-4. We find reasonable one-to-one correspondence as shown in SI-9, between the two sets of plots, in terms of the separation of the spatial distributions of RFs and the COMs of loops-3 and 4. This implies that the RFs get separated along the cell long axis as the Loops-3 and 4 often occupy different regions. This may be a consequence of mutual repulsion between Loops-3 and 4, and further entropic interactions with Loops-1 and 2 of both the replicated chromosomes. All loops jostle for space to avoid each other and often end up interchanging positions.

The reader may question: If the above reasoning is correct then why do the spatial distributions of the RFs in the  $(0.2 - 0.4)$  interval (and in the subsequent intervals except the last one) not show four peaks? We remind the reader that in these stages of the life cycle the RFs mostly traverse along the contours of Loop-1 and Loop-2. They reach Loops 3 and 4 only in the last stage of the life cycle. The Loops-3 and Loop-4 are different from Loops 1 and 2, since they are closer to the *dif-ter* CL along the loop contour. As a consequence Loops 3 and 4 have a greater propensity to interchange positions (to avoid spatial overlaps while exploring conformational microstates) along the cell long axis, as compared to that of loops 1 and 2. The interchanging of loops are better visualised in SI-10. To have a complete understanding of the cause of repulsion between loops, and how the location of the loops along chain contour affects the organization of loops with respect to each other, refer (32).

The spatial location of each locus as they get (replicated and subsequently) separated from its copy was studied in experiments (20). The distribution of these positions along the long-axis for each locus is reproduced in Fig.5(b) for the aid of the reader. We can also obtain this distribution of "position of split" from our simulations, and we show it in SI-11 to see a good match with experiments for certain loci. In SI-11, we further discuss why the 'split positions' of some loci as obtained by us differ from that seen in experiments.

**Data normalization: Experiments vs. Simulations:** There are some other caveats to be aware of. In simulations, we never see a pair of distinctly separated peaks of the *ter* loci distributions, as we do not model cell division. However,

the experimental data shows finite probability for two *dif-ter*s, even when the cell is in its  $(0.6 - 0.8)$  stage of life cycle (as deduced from the length of the cell) as well as for the interval  $(0.8 - 1)$ . In experiments, the cell lengths is used as a proxy for age of the cell. These could give rise to discrepancies when analyzing data by image processing softwares.

Moreover, there are differences in the methods of collecting data and normalizing the spatial distributions. In the given experimental data, the cells were first differentiated by their cell-size to categorize the age of the cell. For each such category, the number of distinguishable foci in each cell is observed and spatial distribution data corresponding to number of foci observed, they are normalised with respect to the number of cells in each of the sub-categories. The experimental images are unable to discern if the foci belong to the D-chromosome or GD-chromosome. Furthermore, if the foci cannot be spatially resolved, a 4-foci cell may be erroneously categorized as a three-foci or a two-foci cell. The three foci scenario may also arise due to asynchrony in the replication initiation process or stochasticity in the cohesion times. In the simulations we do not have asynchrony in the replication initiation process, however, there maybe stochasticity in the cohesion times of the loci. But, we have access to the positions of each monomers at all stages of the simulation run. Thus, our normalization protocol is different to that adopted in experiments.

In simulations, we have 50 independent runs to collect data over the entire life cycle, and thereby precisely know the stage of the life-cycle, when a loci is replicated to two loci of the next generation. We thereby normalize by the precise number of micro-states relevant for a particular monomer, depending on when that monomer has been introduced within that interval of the life cycle. For each independent run having a total of  $5 \times 10^7$  MCS, we store data to calculate distributions every  $3 \times 10^4$  MCS. Thereby, we know the number of contributing micro states in each stage of of the life cycle for each loci.

**Spatial distribution of other loci:** We now look at the spatial distributions of the other tagged loci in the experiments. We check whether we obtain distributions similar to those obtained by (20), relevant data has been reproduced in Fig.5 for comparison. Here we provide data for five such loci from the left arm in Fig.7 (as in (20)). The data for the loci on the right arm are given in SI-12.

For the locus marked as 54.2' (monomer 150), we see only two distributions for  $(0 - 0.8)$  intervals of the life cycle, as the monomers of the daughter chromosomes get replicated only at the end of the fourth interval. Our modeling data is in fair agreement with the experimental data. We find that there are four peaks towards the end of the life cycle. Experimentally, it is not possible to distinguish between the two GD loci near the end of the life cycle, as they cannot be spatially resolved if are spatially proximal. In our simulations, we can uniquely identify the loci of each GD chromosome, and thereby, we obtain four distinct spatial distributions, albeit they overlap. In experiments, the loci distributions (that we obtain) will appear as broad distributions having only two distinct peaks. In this sense, our spatial distribution of loci are in agreement with the experimentally obtained distributions (20).

The data obtained from simulations for the locus marked as 45.1' (monomer 200) also shows good agreement with the experimental data for 2 foci. We do not have four peaks for this locus in the  $(0.8 - 1)$  interval since the simulations are stopped

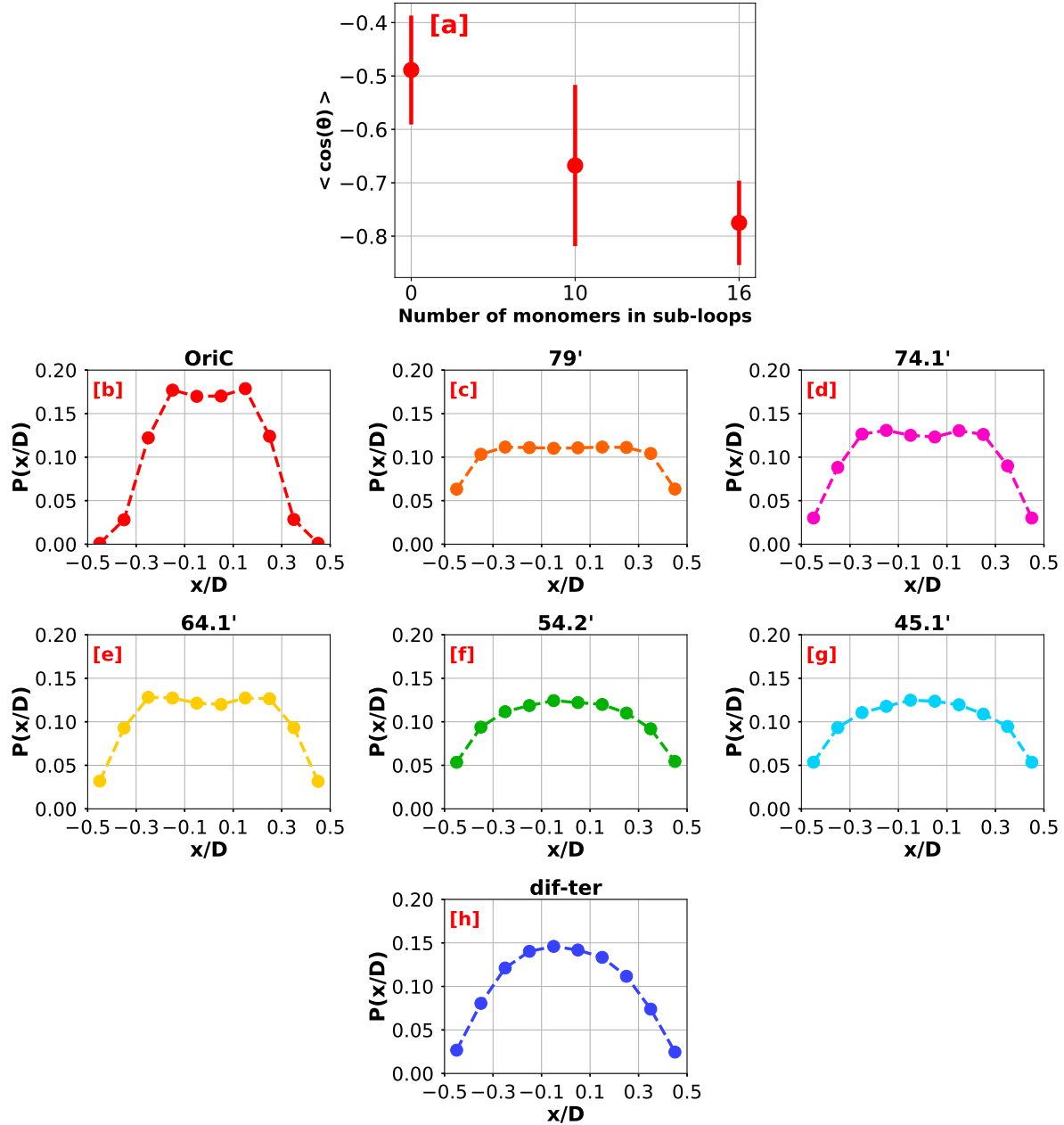


**Fig. 8. Radial organization of arms and radial distribution of loci:** Subfigure (a) shows  $\langle \cos(\theta) \rangle$ , where  $\theta$  denotes the angle between vectors  $\vec{l}_1$  and  $\vec{l}_2$  (refer text). A high negative value of  $\cos(\theta)$  indicates that the two loops (belonging to the two arms of the chromosome) lie on different cell halves along the radial axis. We have computed the average value of  $\cos(\theta)$  by considering 1000 microstates. We observe that the average  $\cos\theta$  value is more negative in the cases with smaller loops (within Loop-1 and Loop-2) as compared to the case without smaller loops. Subfigures(b-h) show the radial probability distributions of the monomers for several loci in the presence of smaller loops. These smaller loops are of size 10 monomers each and are placed along loop-1 and loop-2. We show here the data for the loci of the left arm, while the corresponding data for the right arm loci have been provided in the Supplementary. We note that we obtain a bimodal distribution for some loci, by the introduction of these smaller loops. The distributions we obtain match those found in the experiments for the loci *oriC*, 79', 74', 45.1' *dif-ter* along the left arm only. The corresponding data for the loci in the right arm have been provided in SI-15. The experimentally obtained radial distributions for the loci have also been reproduced in SI-16 for aid of comparison. We do not obtain a match for the locus 54.2' and data for some other loci on the right arm (presented in SI). We also notice that we obtain a double peaked distribution of the *oriC* while the experimentally obtained distribution has a single peaked distribution. However, we have explicitly checked that one can obtain an exact match with experiments by tuning the size and location of these loops along the chain contour. But this is outside the scope of this study. Here we have just established the mechanism by which one may obtain the bimodal peaks in the radial distribution plots of genomic loci.

just as this specific locus gets replicated. Correspondingly, the experimental data also doesn't have any contribution from this locus in the  $(0.8 - 1)$  interval, for the row with 4 foci. Furthermore, comparing our data in other intervals with the 2 foci data in Fig.5, the distribution of the locus 45.1' is peaked near the center as this locus is close to *dif-ter*. As the cell ages, the loci moves away from each other, hence delocalizing from the center of the cell due to the presence of mutual repulsion between Loop-3 and Loop-4. But once the Loop-1 and Loop-2 of the GD1' and GD2' chains are formed, they are pushed away from the poles in the  $(0.6 - 0.8)$  interval. Thus, our data is consistent with the experimentally obtained data of Fig.5.

In the third row of Fig.7 we show data for the locus 79' (monomer 26). We note that the distributions from our simulations peak around the cell poles. This differs from two foci data from experiments in the  $(0 - 0.4)\tau$  intervals, where they find that this locus is localized around the quarter positions. We have not incorporated the effects of transient loops in the current work. We presume that if we introduce transient loops in our simulations, this locus will stay away from the poles. This is because loops maintain distance from the walls to entropically explore conformations and can lead to better match with experimental data. In later parts of the cell-cycle with more than two foci, the experimental distribution is broad, and four peaks are observed. We do have distributions which are spread out over the length of the cell. But we obtain a reasonable match with experimental data only in the  $(0.8 - 1)\tau$  interval as there are peaks around the quarter positions and at the poles.

We may reason along similar lines as to why the distributions obtained for the 74' locus is different to those seen in experiments. This locus again lies within the Loop-1, and would remain away from the cell-center (where the *dif-ter* is located). While there are broad similarities between the two sets of data, we still have high probability to obtain the loci right at the poles. This differs from the experimental data.

**Radial distributions of loci:** Reference (20) also provides experimental data for the radial distributions of loci along the radial axes, i.e. directions perpendicular to the long axis of the cylinder (say the  $z$  axis). We plot spatial distributions using the  $x$  or  $y$  coordinate of the loci as both of these can be referred to as "radial" directions, refer Figures in SI-13 and SI-14. We find that these distributions show in general broad distributions peaked at the middle of the cylinder, while the experimental data show doubled peaked distribution for some loci.

We propose an outline of the mechanism by which one can obtain such bimodal distribution as seen in experiments. A suitable modification of the the simple Arc-2-2 architecture results in the bimodal distribution of monomers (loci). We introduce 6 smaller subloops in each of Loop-1 and Loop-2 of size 10 monomers each. These subloops are equally spaced with 10 monomers in between. The introduction of these subloops enhances the entropic repulsion between Loop-1 and Loop-2 along the short axis. As a consequence, the monomers belonging to those loops show a bimodal distribution. We show this through simulations of two Arc-2-2 polymers segregated in space, with subloops of size 10 monomers in Loop-1 and Loop-2. We do not incorporate replication, since we only outline the mechanism by which one may obtain such bimodal distributions. The existence of topologically associated do-

main(TADs) in Hi-C maps indicate the existence of smaller loops in the DNA-polymer (35–47). We take equally sized and spaced subloops as a simple proof-of-concept model to establish that the smaller loops help in the radial organization of the loci. These loops will appear to be transient *in-vivo*.

To establish that Loop-1 and Loop-2 lie in different halves of the cylinder, along the radial axis, we carry out the following calculation. We construct a vector  $\vec{l}_1$  joining the mid-point of the cylinder and the COM (center of mass) of Loop-1. Similarly, we construct another vector  $\vec{l}_2$  joining the center of the cylinder and the COM of Loop-2. Note that we only consider the  $\hat{x}$  and  $\hat{y}$  components of the vectors. The angle between the two vectors is denoted by  $\theta$ . Then, if  $\cos\theta \approx -1$ , the two vectors are anti-parallel to each other. This implies that the two loops, Loop-1 and Loop-2 (belonging to different arms of the chromosome) lie in different cell halves along the short axis. As can be inferred from Fig.8(a), we observe that introduction of smaller additional loops leads to the separation of arms along the short axis. We further note in Fig.8(b-h) that the introduction of subloops also leads to bimodal distributions of some loci along short axis, similar to what is seen in (20). Other loci show broader radial distributions as compared to radial distributions for Arc-2-2 polymers without smaller loops (refer SI-13 & SI-14), even if they do not show bimodal distributions. To check for robustness of our conclusions, we conduct similar simulations with five smaller subloops within Loop-1 (and Loop-2) with 16 monomers in each of the subloops. This also shows separation of these arms as can be inferred from values of  $\langle \cos(\theta) \rangle$ , refer Fig.8(a). This however fails to show bimodal radial distribution.

Furthermore, one may also introduce smaller loops along the rest of the Arc-2-2 polymer (outside loop-1 and loop-2) to obtain the bimodal distribution of other monomers. In the experimental data of (20), some loci show single peaked distributions while others show bimodal distribution. Even in our simulations, some monomers show single peaked distributions while others show bimodal distributions, although an exact match is not obtained with experiments. To obtain an exact match one needs to optimize the size and location of loops along the contour, which is out of the scope of the current manuscript.

## 2. Discussion

We establish that entropic repulsion between loops is a viable mechanism through which the chromosomes segregate and organise themselves. We show that the organisation of *oriC*, *dif-ter* and other loci emerge spontaneously in our model, both along the longitudinal and the radial axis. Our model also successfully reconciles other experimental observations such as the spatial organization of replication forks. We have also shown that even though we have modeled the replication process in a train-track manner, the adoption of a particular polymer architecture by the chromosome results in the localisation of the RFs which supports (in spirit) the replication-factory model. Thus, the hypothesis first proposed by the authors of (20): "The position and dynamics of the replication forks are likely the consequence of the spatial organization of the chromosomes rather than vice-versa" is justified and the mechanism has been established by us. With this work and our past paper on the organization of *E.coli* chromosomes in slow growth conditions using the Arc-2-2 architecture (31), we present a

unified model of the *E. coli* chromosome organization for all growth conditions.

Although our coarse-grained model is able to reconcile multiple experimental results, the model still has room for improvement in the future. The incorporation of crowders in our model (23, 48, 49) could condense the chromosome significantly and away from the cylinder-ends. One may also incorporate effects of other transient cross-links in addition to the permanent (long-lived) cross-links that we have employed. Binding and loop extrusion proteins, which associate and disassociate from the chromosome at different stages of the cell-cycle, are likely to result in transient cross-links and further fine-tune evolution of organization. We mimic the action of the Topoisomerase enzymes by decreasing the monomer-diameters at infrequent but regular intervals. This enzyme acts *in vivo*, to remove topological constraints locally along the chain contour. In our study, we use Monte Carlo simulations to realize local diffusion of polymer segments within a confining cylinder (cell), which results in emergent entropic repulsion between different loops of the DNA-polymer. Consequently, we obtain evolution of organization of the chromosome, though we have a non-equilibrium system.

We have outlined principles by which one may obtain the experimental data of (20) though our model of the DNA-polymer with a modified topology. The experiments were conducted on a specific growth medium of the bacterial cells, which determines the value of  $\tau_C$ ,  $\tau_D$  and the doubling time. We have adapted our model similarly to establish a correspondence to the experiments of (20). In future manuscripts, we shall communicate our results for a different choice of  $\tau_C$ ,  $\tau_D$ , and the doubling time. We hope that our theoretical predictions can then be validated by experiments conducted using different growth media.

### 3. Acknowledgements

Authors acknowledge useful discussions with Arieh Zaritsky, Conrad Woldringh, Tejal Agarwal and Suckjoon Jun. A.C., with DST-SERB identification SQUID-1973-AC-4067, acknowledges funding by DST-India, project MTR/2019/000078 and CRG/2021/007824. A.C also acknowledges discussions in meetings organized by ICTS, Bangalore.

- R Phillips, J Kondev, J Theriot, HG Garcia, N Orme, *Physical Biology of the Cell*. (Garland Science), (2012).
- A Kuzminov, The chromosome cycle of prokaryotes. *Mol. Microbiol.* **90**, 214–227 (2013).
- JK Fisher, et al., Four-dimensional imaging of *e. coli* nucleoid organization and dynamics in living cells. *Cell* **153**, 882–895 (2013).
- L Dewachter, N Verstraeten, M Fauvart, J Michiels, An integrative view of cell cycle control in *escherichia coli*. *FEMS Microbiol. Rev.* **42**, 116–136 (2018).
- A Japaridze, C Gogou, JWW Kerssemakers, HM Nguyen, C Dekker, Direct observation of independently moving replisomes in *escherichia coli*. *Nat. Commun.* **11** (2020).
- J Mäkelä, DJ Sherratt, Organization of the *escherichia coli* chromosome by a MukBEF axial core. *Mol. Cell* **78**, 250–260.e5 (2020).
- SM Mangiameli, JA Cass, H Merrikh, PA Wiggins, The bacterial replisome has factory-like localization. *Curr. Genet.* **64**, 1029–1036 (2018).
- A Badrinarayanan, TB Le, MT Laub, Bacterial chromosome organization and segregation. *Annu. Rev. Cell Dev. Biol.* **31**, 171–199 (2015).
- CL Woldringh, N Nanninga, Structural and physical aspects of bacterial chromosome segregation. *J. Struct. Biol.* **156**, 273–283 (2006).
- S Ben-Yehuda, RacA, a bacterial protein that anchors chromosomes to the cell poles. *Science* **299**, 532–536 (2002).
- C Gogou, A Japaridze, C Dekker, Mechanisms for chromosome segregation in bacteria. *Front. Microbiol.* **12**, 1533 (2021).
- S Jun, A Wright, Entropy as the driver of chromosome segregation. *Nat. Rev. Microbiol.* **8**, 600–607 (2010).
- JJB Messelink, MCF van Teeseling, J Janssen, M Thanbichler, CP Broedersz, Learning the distribution of single-cell chromosome conformations in bacteria reveals emergent order across genomic scales. *Nat. Commun.* **12** (2021).
- PH Viollier, et al., Rapid and sequential movement of individual chromosomal loci to specific subcellular locations during bacterial DNA replication. *Proc. Natl. Acad. Sci.* **101**, 9257–9262 (2004).
- SM Mangiameli, BT Veit, H Merrikh, PA Wiggins, The replisomes remain spatially proximal throughout the cell cycle in bacteria. *PLOS Genet.* **13**, e1006582 (2017).
- HJ Nielsen, Y Li, B Youngren, FG Hansen, S Austin, Progressive segregation of the *escherichia coli* chromosome. *Mol. microbiology* **61**, 383–393 (2006).
- JF Marko, Linking topology of tethered polymer rings with applications to chromosome segregation and estimation of the knotting length. *Phys. Rev. E* **79**, 051905 (2009).
- C Helmstetter, S Cooper, O Pierucci, E Revelas, On the bacterial life sequence. *Cold Spring Harb. Symp. on Quant. Biol.* **33**, 809–822 (1968).
- A Zaritsky, W Vollmer, J Männik, C Liu, Does the nucleoid determine cell dimensions in *escherichia coli*? *Front. Microbiol.* **10** (2019).
- B Youngren, HJ Nielsen, S Jun, S Austin, The multifork *escherichia coli* chromosome is a self-duplicating and self-segregating thermodynamic ring polymer. *Genes & Dev.* **28**, 71–84 (2014).
- S Jun, B Mulder, Entropy-driven spatial organization of highly confined polymers: Lessons for the bacterial chromosome. *Proc. Natl. Acad. Sci.* **103**, 12388–12393 (2006).
- S Jun, A Arnold, BY Ha, Confined space and effective interactions of multiple self-avoiding chains. *Phys. Rev. Lett.* **98** (2007).
- J Pelletier, et al., Physical manipulation of the *escherichia coli* chromosome reveals its soft nature. *Proc. Natl. Acad. Sci.* **109**, E2649–E2656 (2012).
- Y Jung, BY Ha, Overlapping two self-avoiding polymers in a closed cylindrical pore: Implications for chromosome segregation in a bacterial cell. *Phys. Rev. E* **82**, 051926 (2010).
- Y Jung, et al., Ring polymers as model bacterial chromosomes: confinement, chain topology, single chain statistics, and how they interact. *Soft Matter* **8**, 2095–2102 (2012).
- Y Jung, J Kim, S Jun, BY Ha, Intrachain ordering and segregation of polymers under confinement. *Macromolecules* **45**, 3256–3262 (2012).
- BY Ha, Y Jung, Polymers under confinement: single polymers, how they interact, and as model chromosomes. *Soft Matter* **11**, 2333–2352 (2015).
- VS Lioy, I Junier, F Boccard, Multiscale dynamic structuring of bacterial chromosomes. *Annu. Rev. Microbiol.* **75** (2021).
- J Cass, N Kuwada, B Traxler, P Wiggins, *Escherichia coli* chromosomal loci segregate from midcell with universal dynamics. *Biophys. J.* **110**, 2597–2609 (2016).
- CL Woldringh, FG Hansen, NOE Vischer, T Atlung, Segregation of chromosome arms in growing and non-growing *escherichia coli* cells. *Front. Microbiol.* **6** (2015).
- D Mitra, S Pande, A Chatterji, Polymer architecture orchestrates the segregation and spatial organization of replicating *e. coli* chromosomes in slow growth. *Soft Matter* **18**, 5615–5631 (2022).
- D Mitra, S Pande, A Chatterji, Topology-driven spatial organization of ring polymers under confinement. *Phys. Rev. E* **106**, 054502 (2022).
- K Kikuchi, M Yoshida, T Maekawa, H Watanabe, Metropolis monte carlo method as a numerical technique to solve the fokker–planck equation. *Chem. Phys. Lett.* **185**, 335–338 (1991).
- SC Glotzer, D Stauffer, N Jan, Monte carlo simulations of phase separation in chemically reactive binary mixtures. *Phys. Rev. Lett.* **72**, 4109–4112 (1994).
- A Hofmann, DW Heermann, The role of loops on the order of eukaryotes and prokaryotes. *FEBS Lett.* **589**, 2958–2965 (2015).
- VS Lioy, et al., Multiscale structuring of the *e. coli* chromosome by nucleoid-associated and condensin proteins. *Cell* **172**, 771–783.e18 (2018).
- TB Le, MT Laub, New approaches to understanding the spatial organization of bacterial genomes. *Curr. Opin. Microbiol.* **22**, 15–21 (2014).
- TBK Le, MV Imakaev, LA Mirny, MT Laub, High-resolution mapping of the spatial organization of a bacterial chromosome. *Science* **342**, 731–734 (2013).
- MA Umbarger, et al., The three-dimensional architecture of a bacterial genome and its alteration by genetic perturbation. *Mol. Cell* **44**, 252–264 (2011).
- A Maji, R Padinhateeri, MK Mitra, The accidental ally: Nucleosome barriers can accelerate cohesin-mediated loop formation in chromatin. *Biophys. J.* **119**, 2316–2325 (2020).
- T Agarwal, GP Manjunath, F Habib, A Chatterji, Origin of spatial organization of DNA-polymer in bacterial chromosomes. *EPL (Europhysics Lett.)* **121**, 18004 (2018).
- T Agarwal, GP Manjunath, F Habib, A Chatterji, Bacterial chromosome organization. I. crucial role of release of topological constraints and molecular crowders. *The J. Chem. Phys.* **150**, 144908 (2019).
- T Agarwal, GP Manjunath, F Habib, A Chatterji, Bacterial chromosome organization. II. few special cross-links, cell confinement, and molecular crowders play the pivotal roles. *The J. Chem. Phys.* **150**, 144909 (2019).
- A Wasim, A Gupta, J Mondal, A Hi–C data-integrated model elucidates *E. coli* chromosome's multiscale organization at various replication stages. *Nucleic Acids Res.* **49**, 3077–3091 (2021).
- AM Chiariello, C Annunziatella, S Bianco, A Esposito, M Nicodemi, Polymer physics of chromosome large-scale 3d organisation. *Sci. Reports* **6** (2016).
- Q Szabo, et al., TADs are 3d structural units of higher-order chromosome organization in *drosophila*. *Sci. Adv.* **4** (2018).
- S Guha, MK Mitra, Multivalent binding proteins can drive collapse and reswelling of chromatin in confinement. *Soft Matter* **19**, 153–163 (2023).
- M Joyeux, *Compaction of bacterial genomic DNA: clarifying the concepts*. *J. Physics: Condens. Matter* **27**, 383001 (2015).
- M Joyeux, *A segregative phase separation scenario of the formation of the bacterial nucleoid*. *Soft Matter* **14**, 7368–7381 (2018).